

Doubling growth of egg-box structure during Calcium-mediated molecular assembly of alginate

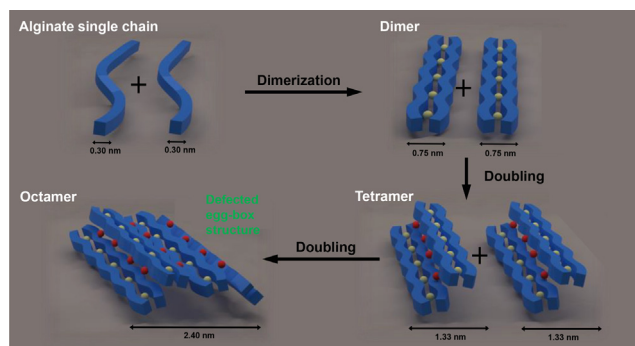


Yi Wang^{a,1}, Yiguo Zhao^{a,1}, Jun He^a, Cuixia Sun^a, Wei Lu^a, Yin Zhang^b, Yapeng Fang^{a,*}

^aSchool of Agriculture and Biology, Shanghai Jiao Tong University, 800 Dongchuan Road, Shanghai 200240, China

^bKey Laboratory of Meat Processing of Sichuan, Chengdu University, Chengdu 610106, China

GRAPHICAL ABSTRACT



ARTICLE INFO

Article history:

Received 7 September 2022

Revised 30 November 2022

Accepted 18 December 2022

Available online 20 December 2022

Keywords:

Alginate

Calcium

Egg-Box Structure

Molecular Assembly

Doubling Growth

ABSTRACT

Ca²⁺-mediated molecular assembly of alginate underpins its wide range of applications in foods, pharmaceuticals, biomedicines, tissue engineering and environmental treatments. The mode of growth of egg-box structure of alginate in the presence of Ca²⁺ is a long-standing fundamental problem to be concluded. In this work, we investigate the Ca-induced structural evolution of alginate in dilute solution using atomic force microscopy and dilute solution viscometry. It is demonstrated that the structural evolution follows the three critical steps of monocomplexation, dimerization and multimerization, upon binding with Ca²⁺. Interestingly, the alginate single chains grow into dimers and multimers via a doubling mode, i.e., successive emerging of dimer, tetramer, octamer, and hexadecamer. Compared with lower guluronate (G) alginate, higher G alginate exhibits a more pronounced multimerization process occurring at a lower ratio of Ca/G. A mechanistic model depicting the evolution of egg-box structure is proposed. The results would add new knowledge to the current egg-box model regarding the molecular assembly and gelation of an important biopolymer alginate, and provide fundamental basis for molecular engineering of alginate for more advanced applications.

© 2022 Elsevier Inc. All rights reserved.

1. Introduction

Alginate is an important natural polysaccharide produced from brown seaweeds and some bacteria [1]. It is composed of linearly (1 → 4)-linked β-D-mannuronate (M) and α-L-guluronate (G) residues arranged in a blockwise pattern including G-blocks,

* Corresponding author.

E-mail address: ypfang@sjtu.edu.cn (Y. Fang).

¹ These authors contributed equally.

M-blocks and MG-blocks [2]. The overall composition of M/G residues and their distribution pattern greatly impact on the properties and functionalities of alginate. Being edible, biocompatible, biodegradable, and environment-friendly, alginate has found numerous applications in the food, cosmetic, pharmaceutical, biomedical and environmental industries [3]. Most of the applications are based on the binding, assembling and gelling ability of alginate in the presence of divalent cations, particularly, Ca^{2+} ions. An in-depth understanding of the Ca^{2+} -mediated assembly of alginate is thus of utmost importance for expanding more advanced utilizations.

The famous egg-box model, originally proposed by Rees et al., has been regarded as a classic mechanism to depict the molecular assembly of alginate with Ca^{2+} [4–6]. In the model, two oppositely facing G sequences pair together to form buckled structure possessing cavities, within which Ca^{2+} ions are accommodated through specific coordination interaction. This results in cross-linked dimers with geometric structure that resembles egg-box. In the presence of sufficient Ca^{2+} , the dimers can further aggregate laterally into multimers, as revealed by small angle X-ray scattering [7,8]. Through analysis of crystal structure, Sikorski et al. proposed that the lateral aggregation is most likely to be mediated by nonspecific interactions involving Ca^{2+} , Na^+ and H_2O , forming defected yet egg-box-compatible structure [9].

In contrast to the static structural studies, limited research has been conducted to elucidate the dynamic process of structural evaluation during the egg-box formation. Our early studies using isothermal titration calorimetry and viscometry found that the formation of egg-box structure involves three distinct and successive steps, i.e., monocomplexation, dimerization and multimerization [10,11]. The dimerization is a rather critical process of chain pairing, starting from at $\text{Ca}/\text{G} = 0.25$. The multimerization however is a less critical process with a broader transition, happening via lateral aggregation of dimers when $\text{Ca}/\text{G} > 0.55$. By means of viscometry, light scattering, circular dichroism, and fluorescence quenching, Donati et al. proposed a tilted egg-box model to challenge the monocomplexation step [12]. They argued that the initial binding of Ca^{2+} at $\text{Ca}/\text{G} < 0.25$ can also cause the crosslinking of alginate chains, leading to the formation of tilted egg-box structure. The tilted egg-box model was further interpreted using another polyuronate pectin within the framework of modified counterion condensation theory [13]. The tilted egg-box model seems impossible, as recent evidence shows no gelation for concentrated alginate solutions at $\text{Ca}/\text{G} < 0.25$. This directly disproves the presence of tilted egg-box crosslinking, which otherwise would cause alginate gelation [14,15]. A recent computational modeling of alginate gelation based on the discrete element method (DEM) also demonstrated that a critical value of Ca/G is required for the crosslinking and gelation of alginate [16]. The tilted egg-box at most is a type of loosely bound and transient cross-links that are formed in equilibrium with monocomplexes [15]. Moreover, local overconcentration of Ca^{2+} during inhomogeneous mixing with alginate may also be accountable for chain crosslinking at the initial binding stage of $\text{Ca}/\text{G} < 0.25$, as observed by Donati et al [12]. Therefore, a detailed and conclusive analysis of the dynamic evolution of egg-box structure during Ca^{2+} -mediated molecular assembly of alginate is required to answer the long-lasting debated issue.

Atomic force microscopy (AFM) has proven to be a powerful tool to realize single molecule imaging. Recent advances in AFM technique, particularly, the use of high-resolution AFM in combination with polymer statistical analysis, allows detailed structural transition and formation of hierarchical structure to be elucidated at molecular level for several polysaccharides [17–20]. For instance, Mezzenga et al. unraveled unambiguously by AFM that the ordered conformation in iota-carrageenan exists as a unimeric helix formed intramolecularly by a single polysaccharide chain

[17]. As in the case of proteins, polysaccharides such as kappa-carrageenan and low acetyl gellan were also found to exhibit multiple structural levels, i.e., primary, secondary, tertiary and quaternary structure, upon addition of specific cations [19,20]. Considerable effort has been made to investigate the molecular assembly and structural evolution of alginate mediated by Ca^{2+} in relation to gelation [21,22]. It was demonstrated that pairs of at least eight G residues are required to form a strong and stable egg-box structure [23]. Additionally, alginate assembly at network level has been visualized and related structural and mechanical characteristics reported [24]. However, due to limited resolution and high working concentration of alginate, the previous studies failed to resolve the evolution of egg-box structure quantitatively at molecular level. Here, we employ AFM and viscometry to examine the molecular assembly and egg-box formation of alginate upon addition of Ca^{2+} . Statistical analysis on AFM images provides a clear picture and quantitative information on the pathway and mode of chain growth from single molecule to dimers and further into multimers.

2. Experimental section

2.1. Materials

Two sodium-type alginates with nominal higher and lower guluronate (G) content were obtained from San Ei-Gen FFI Inc. (Osaka, Japan) and Macklin Inc. (Shanghai, China), respectively. Calcium chloride dihydrate ($\text{CaCl}_2 \cdot \text{H}_2\text{O}$) and sodium acetate (CH_3COONa) of analytical grade were purchased from Sinopharm Chemical Reagent Co., Ltd. (China), whereas 3 Aminopropyl triethoxysilane (APTES, CAS91930-2, 99%) was obtained from Beijing InnoChem Science and Technology Co., Ltd (China).

Alginate samples were purified by extensive dialysis against Milli-Q water to remove free salts before uses. The major cation contained in the samples is sodium ion, and the other cations such as K^+ , Ca^{2+} and Mg^{2+} are all below 500 ppm, as measured by inductively coupled plasma optical emission spectrometer (ICP-OES, iCAP 7600, Thermo Scientific). Gel permeation chromatography coupled with multi-angle laser light scattering (GPC-MALLS, Viscotek TDAmix, Malvern) and ^1H -nuclear magnetic resonance (^1H NMR, Avance 700 MHz, Bruker) were used to characterize the molecular weight and the M/G content of the samples [14,25]. For GPC-MALLS measurements, 0.2 M aqueous NaCl solution containing 0.005 % NaN_3 was used as eluent. A refractive index increment value (dn/dc) of 0.150 mL/g was used for analysis [14]. For ^1H NMR measurements, the alginate samples were slightly degraded by mild acid hydrolysis, followed by chelation of possible divalent cations using ethylene diamine tetraacetic acid (EDTA) [14,25]. The obtained NMR spectra and related assignments are shown in the Supporting Information Figure S1. The relevant molecular and structural parameters are listed in Table 1. The two alginate samples are designated ALG56 and ALG25, respectively, where the numerical postfix represents the guluronate content in percentage.

3. Relative viscosity measurements

The change of relative viscosity of dilute alginate solution upon addition of CaCl_2 was measured at 25 °C to reflect the evolution of molecular hydrodynamic size during Ca^{2+} -induced assembly of alginate chains.[10] Alginate solution (0.5 mg/mL) was prepared by dispersing in 20 mM acetate buffer (pH 5) with gentle shaking overnight to ensure complete dissolution. 10 mM CaCl_2 solution was prepared using the same buffer solvent. 10 mL of 0.5 mg/mL alginate was pipetted into an Ubbelohde-type capillary viscometer, to which 50 μL of 10 mM CaCl_2 was added stepwise and mixed

Table 1
Molecular and structural parameters of alginate samples.

Sample	M_w (kDa)	M_w/M_n	R_g (nm)	Molar fractions of monomers, diads, and triads ^a								
				F_G	F_M	F_{GG}	F_{GM}	F_{MM}	F_{GGG}	F_{GGM}	F_{MGM}	$N_{G>1}$
ALG56	225	1.23	66.6	0.560	0.440	0.451	0.109	0.307	0.414	0.049	0.059	10
ALG25	226	1.16	67.6	0.247	0.753	0.127	0.120	0.530	0.103	0.025	0.095	6

^a Molar fractions of monomers, diads and triads were calculated from NMR spectra (Figure S1) according to the method reported by Grasdalen et al. [25]. The average length of G blocks larger than one was obtained from the equation: $N_{G>1} = (F_G - F_{MGM})/F_{GGM}$ [14].

extensively by shaking. No gelation occurred in such dilution alginate solutions. The relative viscosity (η_r) was measured after each step of addition of CaCl_2 by recording the flow time of solution:

$$\eta_r = t_s/t_0 \quad (1)$$

where t_s is the flow time of sample solution, and t_0 is the flow time of buffer solvent. Considering the dilution effect introduced therein, control measurements were carried out, in which acetate buffer instead of CaCl_2 solution was added into alginate solution. Note that the flow time was measured in triplicate and average value was used for calculation.

4. Atomic force microscopy (AFM)

For AFM imaging, alginate and $\text{CaCl}_2\text{-H}_2\text{O}$ were dissolved in Milli-Q water instead of acetate buffer to avoid the interference of excessive salts. Calculated volume of 10 mM CaCl_2 was added into 10 mL of 0.5 mg/mL alginate under constant stirring, to achieve desired values of the ratio of $R = \text{Ca/G}$ (0, 0.10, 0.25, 0.30, 0.40, 0.50, 0.75, 1.00, 1.25). After fully mixing, the solutions were subjected to filtration (0.45 μm) using polyethersulfone filter prior to AFM experiments. To achieve single chain visualization, some of the solutions were further diluted to an alginate concentration of 1 $\mu\text{g/mL}$.

To ensure strong adsorption of alginate chain onto AFM substrate and prevent artificial alignment of polymer chains during drying, mica surface was modified with APTES to obtain a positively charged substrate surface [26]. For this purpose, a cleaved mica surface was incubated with 20 μL of 0.01 % v/v freshly prepared aqueous APTES solution for 30 s, thoroughly rinsed with 5 mL Milli-Q water, and dried with pressurized high-purity nitrogen gas. Aliquots of 20 μL diluted alginate solutions were deposited onto the APTES-modified mica substrate. After 30 s of adsorption, the substrates were rinsed with 200 μL Milli-Q water five times and gently dried with pressurized high-purity nitrogen gas. The obtained samples were stored in a desiccator prior to AFM imaging to prevent possible hydration by atmosphere moisture.

The prepared samples were visualized on a Multimode 8 Scanning Force Microscope (Bruker) covered with an acoustic hood to minimize vibrational noise. The AFM was operated at ambient condition with a controlled humidity (RH < 40 %) in tapping mode. ScanAsyst Air cantilever with a spring constant of 0.4 N/m was used. The cantilever was made of silicon nitride, and has a tip radius of 2 nm, which renders a resolution of ca. 0.1 nm. Surface topology images were acquired continuously at 1 Hz over a scan range of $1 \times 1 \mu\text{m}$ or $2 \times 2 \mu\text{m}$ with a resolution of 1024×1024 pixels. The obtained AFM images were flattened to remove background curvature using the Bruker NanoScope Analysis 1.8 software. No further image processing was conducted.

4.1. Data analysis

From AFM images, the alginate chains were digitized using a specially designed software FiberApp [27] to track the polymer

backbones and to extract the coordinates of their contour. The tracking algorithm was based on open active contours [28]. After AFM images were imported into FiberApp, the surface was removed automatically and the zero level of the z-axis (height information) was set against a background area selected as large as possible where no polymer chains were present [18]. The root mean square surface roughness of a representative background area varied typically from 0.05 to 0.12 nm.

For chain height analysis, a number of at least 200 clearly separated individual chains or chain portions without overlapping were traced and analyzed to guarantee significant statistics. Chain height was averaged along the contour for each of the traced chains [18]. Height histograms were represented as number of chains, n_c , with single chain average height $\langle h_s \rangle$ [17]. Gaussian fittings of the height histograms were performed to yield overall average height $\langle h \rangle$ and standard deviation.

The flexibility of alginate chains was characterized by analyzing the chain persistence length L_p . For this purpose, the polymer chains were traced entirely, including both crossing and overlapping chains. A 2D worm-like chain model was used to calculate L_p as follows:

$$\langle R^2 \rangle = 4L_p(L - 2L_p(1 - \exp(-L/2L_p))) \quad (2)$$

where $\langle R^2 \rangle$ is the average square end-to-end distance of the traced polymer chain and L is the internal contour length between the two end points [29]. For statistical significance, at least 200 alginate chains were selected and traced. The presence of crossing chains or overlapping chains has been shown to have no effect on the value of calculated persistence length [18]. It should be pointed out that the calculation of L_p for single alginate chain was based on individual entire chains, while that for dimer considers only the chain portions with increased height of ~ 0.75 nm, which is typical of dimers as demonstrated below.

5. Results and discussion

5.1. Change of hydrodynamic size of alginate chains during Ca^{2+} -Mediated molecular assembly

Alginate is one of the most representative polyuronates, which has been widely used in many sectors of the industry as gelling agents, thickeners, stabilizers, dietary fibers, sewage-treating agents, and scaffolds in tissue engineering, etc. Many of the applications rely on the assembling, crosslinking, and thus change of hydrodynamic size of alginate upon addition of Ca^{2+} . Fig. 1 displays the variation of hydrodynamic size of alginate by plotting relative viscosity η_r as a function of $R = \text{Ca/G}$. For the higher G alginate ALG56, η_r exhibits a three-step change upon addition of Ca^{2+} . The boundaries of the three steps are located at $R = 0.25$ and 0.55, respectively. This is in perfect agreement with the previous observations reported for two alginates with $G = 64\%$ and 46% [10]. Step I is characterized by a decreasing η_r which is even smaller than that of control sample added with solvent. This implies a reduction in hydrodynamic size of alginate during this step. Step II sees a steep increase in η_r , indicating an abrupt increase in hydrodynamic size

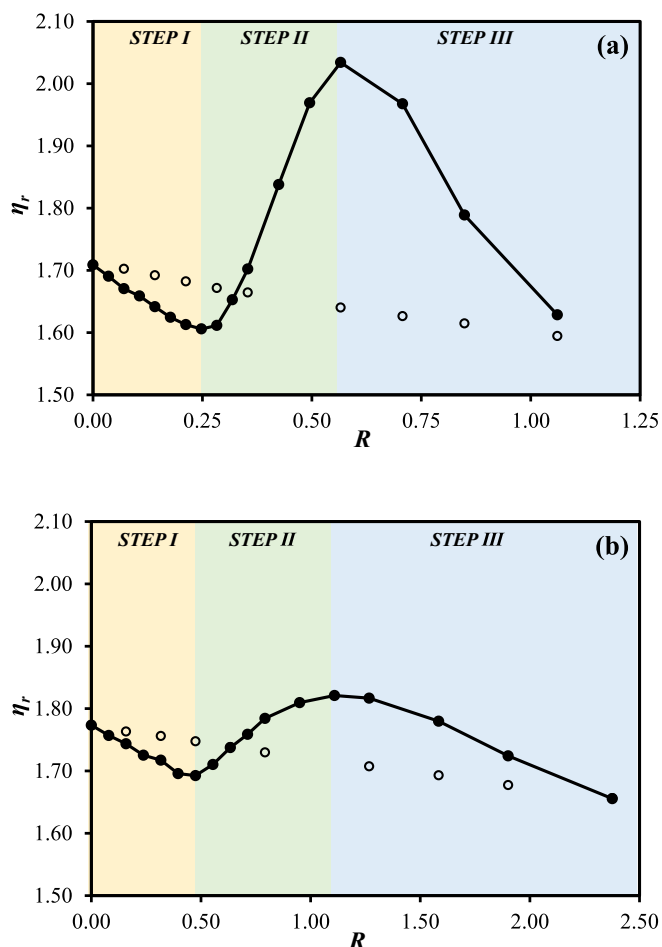


Fig. 1. The change of relative viscosity η_r (solid symbols) with $R = \text{Ca}/\text{G}$ upon addition of 10 mM CaCl_2 into 0.5 mg/mL alginate solution: (a) ALG56; (b) ALG25. The open circles represent control measurements where buffer solvent was added instead of CaCl_2 .

of alginate. Step III is accompanied with a second decrease in η_r , thus a reduction in hydrodynamic size again.

The change of relative viscosity is very sensitive to the hydrodynamic size of alginate chains and thus the molecular assembling under the mediation of Ca^{2+} . Based on the variation in molecular size and in combination with calorimetry during reaction with Ca^{2+} , our previous work proposed a multiple-step mechanism to illustrate this structural evolution of egg-box formation [10,11]. According to the assignments [10,11], Steps I–III are attributed, respectively, to (i) interaction of Ca^{2+} with a single guluronate unit forming monocomplexes, (ii) critical formation and propagation of egg-box dimers via pairing of the monocomplexes, and (iii) lateral association of the dimers creating multimers. The turning points $R = 0.25$ and 0.55 match well with the theoretical stoichiometry of $\text{Ca}/\text{G} = 0.25$ for egg-box dimers and 0.50 for multimers. The small deviation from 0.50 to 0.55 for multimers might be due to the non-specific nature of lateral association mediated not only by Ca^{2+} but also Na^+ , and H_2O etc.[9] The shrinkage of alginate chain due to screened intramolecular electrostatic repulsion upon monocomplexation is responsible for the observed reduction in hydrodynamic size in Step I. It should be mentioned that the reduction in hydrodynamic size in Step I is also partly attributed to increasing ionic strength as Ca is added [18]. However, the electrolyte effect cannot fully explain the reduction, as the effect of adding 10 mM CaCl_2 is much more pronounced than that of adding 20 mM CH_3COONa (control). The abrupt increase in hydrodynamic

size in Step II indicates the critical formation of alginate dimers by chain pairing. The decrease of hydrodynamic size in Step III arises from the collapse of alginate clusters upon multimerization [10,11].

Noteworthy, Donati et al. observed an increased light scattering intensity at initial stage of Ca binding and a shift of the Step I boundary toward lower Ca/G ratio with increasing alginate concentration [12]. They argued for the presence of tilted egg-box crosslinking at $R < 0.25$. The tilted egg-box model however should be disproved, as alginate was demonstrated to be incapable of gelation at $R < 0.25$ in concentrated solutions [14,15]. This is direct evidence ruling out the possibility of the tilted egg-box crosslinking, which otherwise would trigger gelation. Mesoscale modeling of the gelation of alginate based on the discrete element method also identified a critical gelation value of $R \approx 0.26$ for alginate with a very similar guluronate content of 63 % [16]. Relative viscosity and light scattering intensity are very sensitive to the presence of heterogeneous aggregates. The observations by Donati et al. might be attributed to inhomogeneous mixing of alginate with Ca^{2+} , in which local overconcentration of Ca^{2+} would induce local crosslinking and thus dimerization.

Differing from the higher G alginate, ALG25 with a lower G content shows a three-step change of η_r having totally different boundaries, i.e., $R = 0.50$ and 1.10 (Fig. 1b). This indicates that the initiation of dimers and multimers in ALG25 requires double amount of Ca^{2+} in terms of guluronate units, as compared to ALG56. The different stoichiometry could arise from the different modes of Ca^{2+} -mediated assembly of alginate chains. It has been demonstrated that the minimum length of G-blocks required to form a stable egg-box structure must consist of at least 8 consecutive G units. The present alginate samples, ALG56 and ALG 25, possess an average length of G-blocks of 10 and 6 units, respectively, as revealed by NMR structural analysis (Table 1). Therefore, ALG56 can form the classic egg-box junction zones with the stoichiometry of 0.25 and 0.50 for dimers and multimers, respectively. In contrast, the short G-blocks in ALG25 cannot form egg-box-type junction zones, and instead the point-type crosslinks dominated the Ca^{2+} -mediated association of alginate in this case [11,12,15,30]. The formation of point-like crosslinks is related to the relatively random distribution of guluronate units in ALG25. Indeed, the structure of point-type crosslink formed by two G units bridged by one Ca^{2+} ion would yield a stoichiometry of 0.50 that coincides with the observed turning point. Recent molecular modeling of alginate gelation by Depta et al. observed that R value should reach approximately 0.3–0.6 for gelation to occur for a low G alginate with a guluronate content of 33 % [16].

6. Microstructural evolution of alginate chains during Ca^{2+} -Mediated molecular assembly

As forementioned, alginate chains undergo multiple steps of molecular assembly upon addition of Ca^{2+} and give rise to the formation of egg-box structure. These multiple steps have been evidenced indirectly by different physicochemical approaches including viscometry, isothermal titration calorimetry, light scattering, and fluorescence measurements [10,12]. However, there still lacks of proof by direct microstructural observations. The only claimed success was the visualization of the egg-box conformation of calcium alginate by He et al. using negative-staining electron microscopy (EM) [31]. However, due to the cladding effect of the heavy metal stains used for EM sample preparation and the resulting low resolution, it failed to reveal quantitatively the egg-box structure either in terms of structural geometry or stoichiometry. Here, we attempt to provide quantitative insight into the molecular assembly and egg-box formation of alginate upon binding with

Ca^{2+} by means of AFM imaging. To minimize artificial chain alignment and aggregation during sample drying, alginate chains were allowed to adsorb firmly onto AFM substrate by using APTES-modified positively charged mica surface [26]. This AFM imaging protocol was demonstrated capable of reflecting to a large extent the conformation of biopolymers in solutions, and has been successfully applied to the elucidation of conformational transition and hierarchical structure formation for several polysaccharides such as iota-carrageenan, kappa-carrageenan and low acetyl gellan [17–20]. The AFM microstructures represent a two-dimensional thermodynamically equilibrated structure on the AFM substrate surface [32], which allows the statistical analysis and determination of molecular parameters such as chain height and persistence length.

Fig. 2 shows the AFM height images of the higher G alginate ALG56 at a concentration of 0.5 mg/mL and with increasing R , namely, increasing amount of Ca^{2+} . For lower R , e.g., $R = 0.0, 0.10$ and 0.25 , no clear objects were observed on the AFM images. Zooming into the background (marked rectangular area), however, reveals heavily crowding and overlapping of alginate chains. Further dilution to ALG56 = 1.0 $\mu\text{g}/\text{mL}$ gives rise to well-separated single alginate chains, as displayed in Fig. 4 (the first row). Height histograms, represented as number of chains (n_c) with height averaged for each single chain ($\langle h_s \rangle$), shows that the alginate chains belong to the same population with a nearly monomodal Gaussian distribution (the upper right histogram in Fig. 2). It suggests no significant molecular assembly and growth in chain dimension at $R < 0.25$, which corresponds well to the Step I in Fig. 1a. It should be pointed out that the Gaussian distribution of chain height rep-

resents all possible heights measured for different chain configurations and at different locations.

At intermediate values of $R = 0.30, 0.40$ and 0.50 , objects with much larger height (marked by arrows) start to appear on the AFM images. The corresponding height histograms remain monomodal Gaussian distributions. This means that there is still only one population of alginate chains, but with conspicuously larger height of ~ 0.75 nm. The increase in chain height should arise from dimerization of alginate at $0.25 < R < 0.50$, which corresponds to the Step II in Fig. 1a.

When $R > 0.50$, such as $R = 0.75, 1.00$ and 1.25 , AFM images reveal two populations of alginate entities with distinctly different height (marked by solid arrows and broken arrows). The corresponding height histograms exhibit a bimodal Gaussian distribution, and the peaks move toward larger height and tend to be broader with increasing R , indicating a pronounced growth in alginate assembly. This should be in line with the Step III as shown in Fig. 1a.

The evolution of AFM microstructure of the lower G alginate ALG25 with increasing R is displayed in Fig. 3. Differing from ALG56, ALG25 does not show any considerable molecular assembly until up to $R = 0.50$ (no clear objects on AFM height images, the first two rows of Fig. 3). Observation after further dilution to 1.0 $\mu\text{g}/\text{mL}$ demonstrates well-separated single-stranded alginate chains (the second and third rows in Fig. 4). Chain height analysis confirms that the alginate chains belong to the same population with a nearly Gaussian distribution (the right column in Fig. 3). This indicates that no growth in chain dimension happens till to $R = 0.50$, aligning well with the Step I in Fig. 1b.

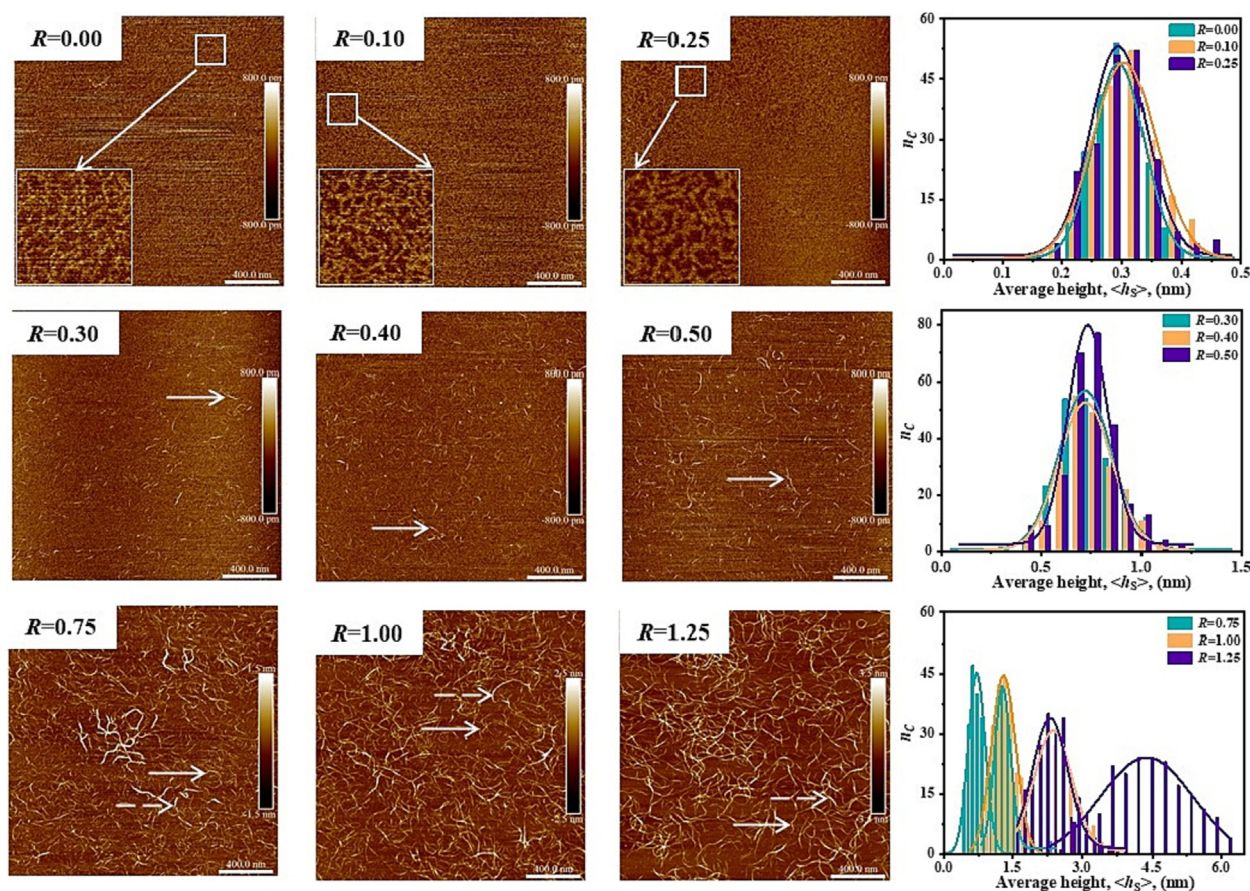


Fig. 2. AFM height images of alginate ALG56 (0.5 mg/mL) at different ratios of $R = \text{Ca}/\text{G}$. The corresponding height histograms with Gaussian fittings (solid lines) are provided on the right side, respectively. The scale bars represent 400 nm. Note that the height histograms for $R = 0.00, 0.10$ and 0.25 were extracted from the AFM height images of further diluted samples (1.0 $\mu\text{g}/\text{mL}$) as shown in Fig. 4.

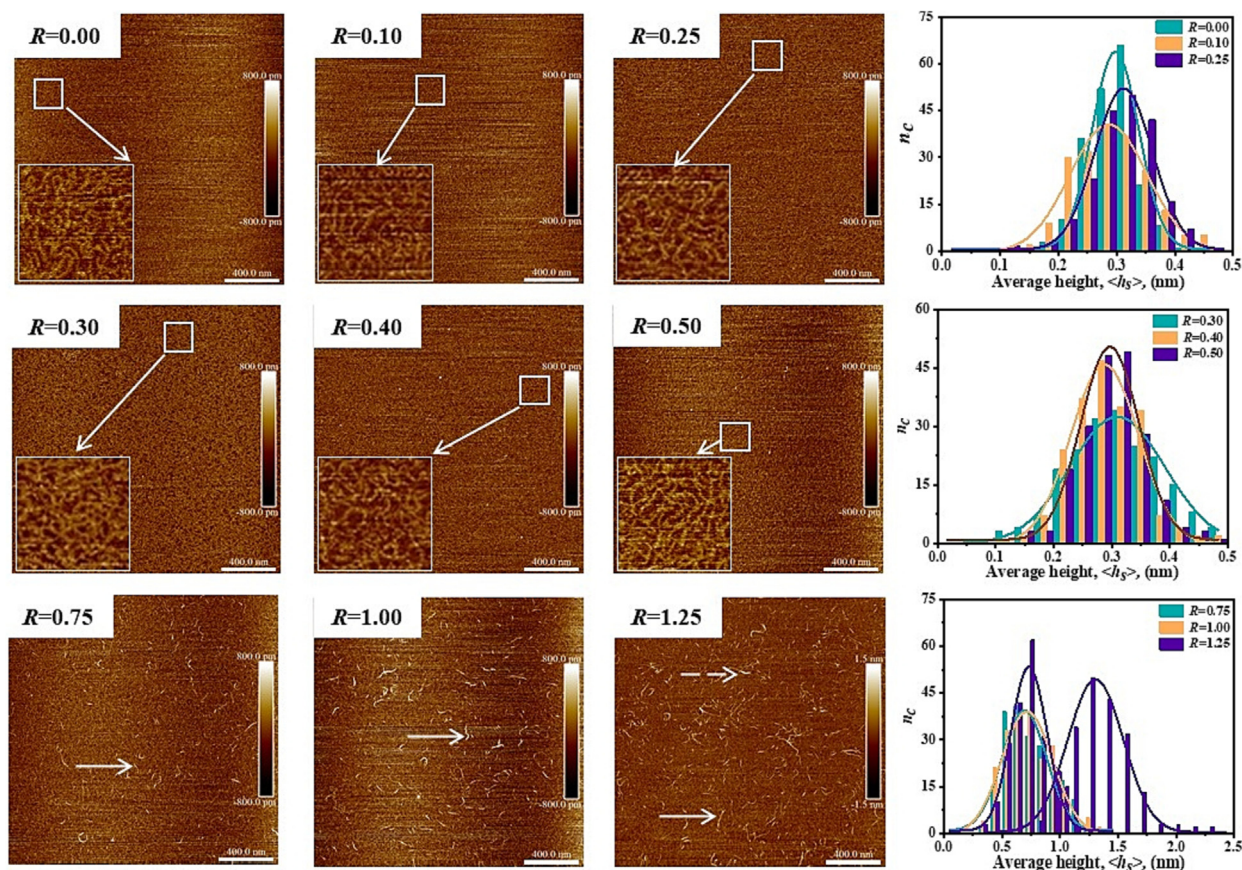


Fig. 3. AFM height images of alginate ALG25 (0.5 mg/mL) at different ratios of $R = \text{Ca}/\text{G}$. The corresponding height histograms with Gaussian fittings (solid lines) are provided on the right side, respectively. The scale bars represent 400 nm. Note that the height histograms for $R = 0.00, 0.10$ and 0.25 were extracted from the AFM height images of further diluted samples (1.0 $\mu\text{g}/\text{mL}$) as shown in Fig. 4.

At intermediate $R = 0.75$ and 1.00 , molecular assemblies with significantly larger height were observed on the AFM images. They belong to the same population with a monomodal Gaussian distribution, as illustrated by the height histograms (the right column in Fig. 3). This stage should correspond to the Step II in Fig. 1b, and is accompanied with a growth in alginate chain dimension. With further increasing R to 1.25 , two populations of alginate assemblies with different heights can be identified (as indicated by the solid arrow and broken arrow). This is more evidenced from the corresponding height histogram, which exhibits a bimodal Gaussian distribution (the right column in Fig. 3). The second peak has a much larger chain height, indicating considerable growth in molecular assembly. This coincides with the Step III shown in Fig. 1b.

The change of alginate chain flexibility upon increasing R was analyzed by calculating the chain persistence length L_p , using the open-source software FiberApp [27]. The curve fittings to the 2D worm-like chain model (eq.2) are displayed in the Supporting Information Figure S2 and S3. Fig. 5 compares L_p versus R for ALG56 and ALG25. The two alginates start with $L_p \approx 26\text{--}29$ nm at $R = 0$. This value is larger than that of ~ 16 nm obtained for alginate in 10 mM NaCl [33–35], and might be attributed to more extended chain conformation at extremely low ionic strength and in 2D space [36]. L_p decreases steadily with increasing R till $R = 0.25$ and 0.50 for ALG56 and ALG25, respectively. The decrease is more significant for ALG56 than that for ALG25. Afterwards, L_p experiences a leap and continues to increase with R . The transition points at $R = 0.25$ and 0.50 match well with those observed in Fig. 1. The initial decrease in L_p should be attributed to the formation of monocomplexes where the binding of Ca^{2+} onto single algi-

nate chains causes the annihilation of negative charges and reduces the intramolecular electrostatic repulsion [37], leading to the decrease in chain stiffness. ALG56 exhibits a larger extent of decrease in chain stiffness simply due to its higher guluronate content. The sudden increase in L_p when R is across 0.25 and 0.50 is related to the dimerization of alginate chains, which gives rise to markedly increased chain stiffness.

7. Growth mode of Egg-Box structure of alginate mediated by Ca^{2+}

The egg-box model is regarded as the most classic mechanism describing the crosslinking and gelation of alginate in the presence of Ca^{2+} . The derivation of the egg-box model was largely based on crystal structural analysis and molecular modeling [9,38–41]. How alginate evolves from single chain to dimer and further to multimer, and the detailed pathway remains unknown and controversial. Here, we discuss the dynamic evolution of alginate egg-box structure and the possible growth mode, by quantitative analysis of the results of AFM microstructures.

Fig. 6 illustrates the evolution of the overall alginate chain height $\langle h \rangle$ with increasing R . $\langle h \rangle$ was taken from the mean of Gaussian fittings of the height histograms in Figs. 2 and 3, and represents the most probable chain height among those measured at different locations and for different chain configurations. It is evident that the evolution of chain height of alginate, either ALG56 or ALG25, upon binding with Ca^{2+} , can be divided into three steps, which are well correlated with the three steps observed in Fig. 1.

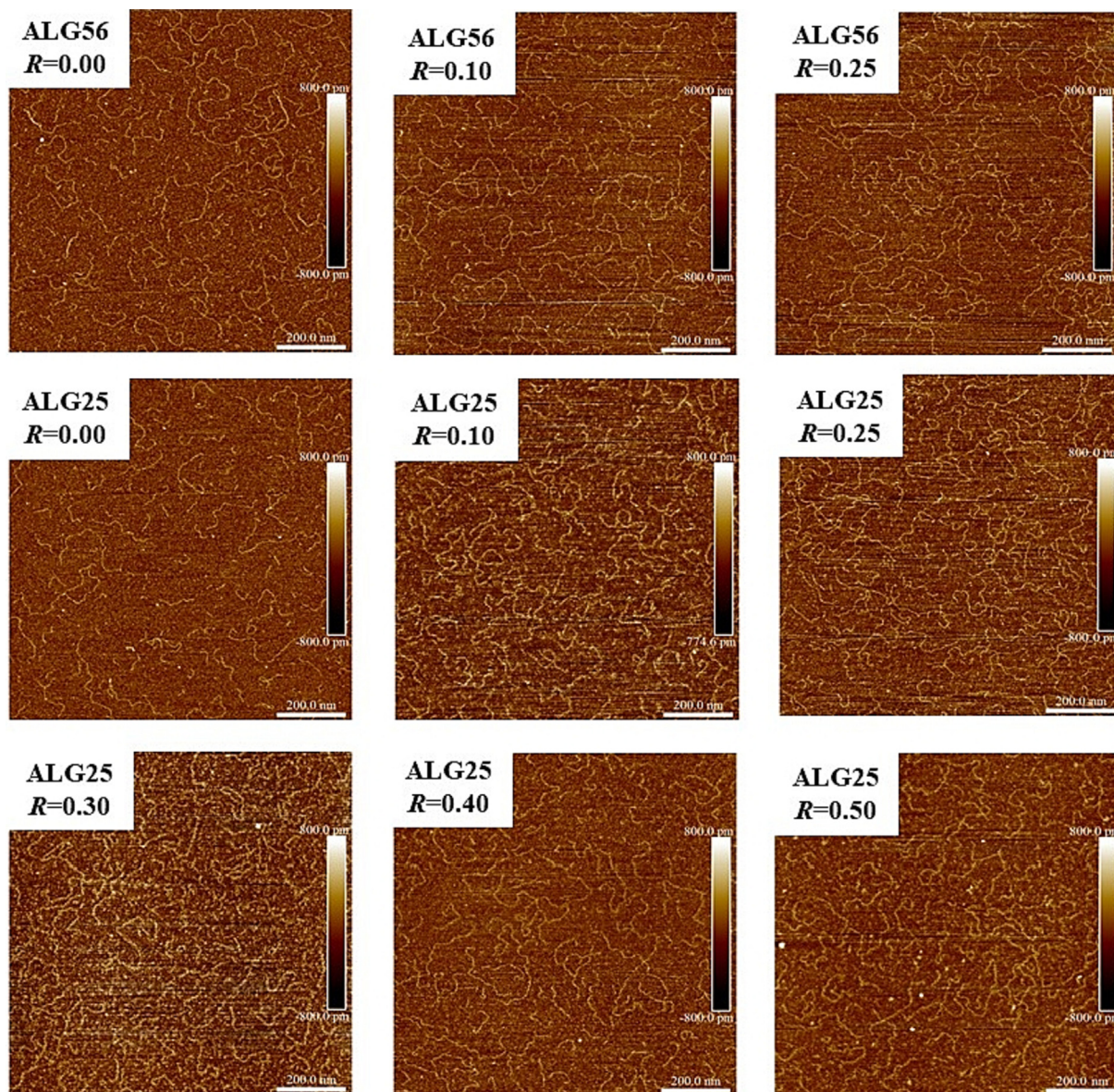


Fig. 4. AFM height images of alginate ALG56 and ALG25 (diluted to 1.0 $\mu\text{g}/\text{mL}$) at different ratios of $R = \text{Ca}/\text{G}$. The scale bars represent 200 nm.

During the Step I (monocomplexation step), i.e., $R < 0.25$ for ALG56 and $R < 0.50$ for ALG25, both alginates show the same and constant chain height of $\langle h \rangle = 0.30$ nm. This should be assigned to single chain alginate without dimerization or crosslinking.[10] The obtained statistical single chain height is smaller than that of 0.43 nm proposed for a single alginate chain packed in a crystal cell.[39] The difference might arise from the restricted and defined configuration of molecular chain within crystal packing. Actually, the maximum measured single chain height (~ 0.45 nm), as demonstrated in height histograms in Figs. 2 and 3, is quite close to the crystallographic single chain width. An early AFM study by Decho et al. reported a much larger single chain height of 1.41–4.65 nm [22]. The author explained the error by the AFM probe-broadening effect and the possible side-by-side association of alginate chains. The incomplete drying of AFM samples at ambient condition, thus a hydrated form, might also contribute to the literature overestimation of the single chain height of alginate.

When $0.25 < R < 0.55$ for ALG56 and $0.50 < R < 1.10$ for ALG25, alginate molecules enter the Step II of dimerization. Both alginates demonstrate a chain height of $\langle h \rangle = 0.75$ nm, which is 2.5 time

that of single chain. Considering the ideal structure of egg-box model, the height or width of N -stranded alginate chain, h_N , can be estimated as follows:

$$h_N = N \times h_1 + (N - 1) \times d_{\text{Ca}} \quad (3)$$

where h_1 is the single chain height of alginate (0.30 nm), and d_{Ca} is the diameter of Ca^{2+} having the value of 0.20 nm [42]. Applying eq. (3) yields a theoretical value of $h_2 = 0.80$ nm for alginate dimers, which is in fairly good agreement with the experimental value of 0.75 nm.

Entering the Step III, i.e., $R > 0.55$ for ALG56 and $R > 1.10$ for ALG25, several distinct values of chain height start to emerge consecutively, e.g., 0.75 nm, 1.33 nm, 2.40 nm, and 4.40 nm. The growth in chain dimension is related to the multimerization of alginate chains as discussed above. Intriguingly, the values of the height follow a strict amplification by 1.8 time, i.e., $1.33/0.75 \approx 1.8$, $2.40/1.33 \approx 1.8$, and $4.40/2.40 \approx 1.8$. Therefore, it is reasonable to assign them to dimer, tetramer, octamer, and hexadecamer, respectively. The results of chain height do not show any clue of the existence of other forms of molecular assemblies,

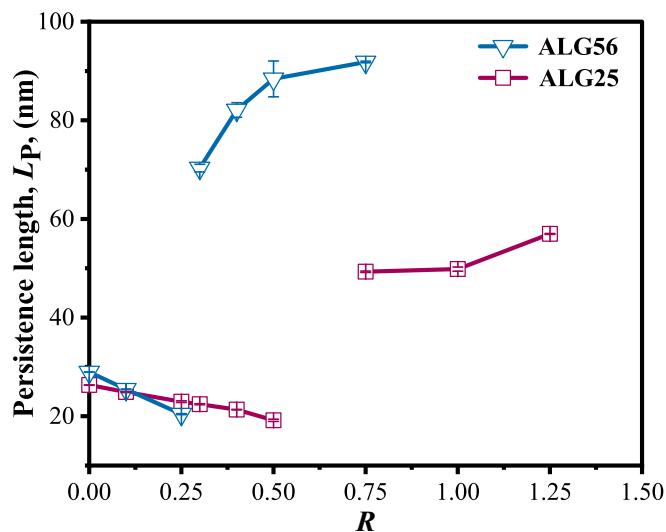


Fig. 5. Variation of chain persistence length L_p with $R = Ca/G$ for ALG56 and ALG25. L_p was calculated according to eq. (2) from AFM image analysis using the open-source software FiberApp [27]. L_p for ALG56 at $R < 0.25$ and ALG25 at $R < 0.50$ was obtained from single chain analysis from Fig. 4, which represents the persistence length of alginate single chains without dimerization. L_p for ALG56 at $R > 0.25$ and ALG25 at $R > 0.50$ was obtained from analysis on chain portions with increased height of ~ 0.75 nm (Fig. 2 and Fig. 3), and therefore represents the persistence length of alginate dimers.

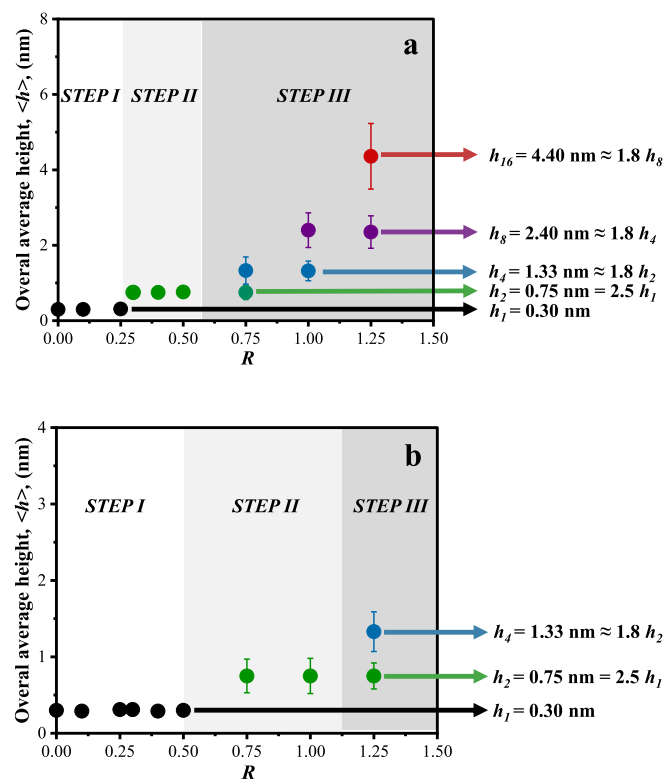


Fig. 6. Plots of the overall average height of alginate chains $\langle h \rangle$ with $R = Ca/G$ for ALG56 (a) and ALG25 (b). $\langle h \rangle$ was obtained from the mean of Gaussian fittings of the height histograms in Fig. 2 and Fig. 3. h_N refers to the height of N -stranded alginate chains, that is, single chain, dimer, tetramer, octamer, and hexadecamer.

i.e., trimer, pentamer, or hexamer. This indicates that the alginate chains grow into egg-box multimers via a doubling mode. The doubling growth mode reflects a cooperative nature of the molecular assembly of alginate in the presence of Ca^{2+} . Furthermore, it can

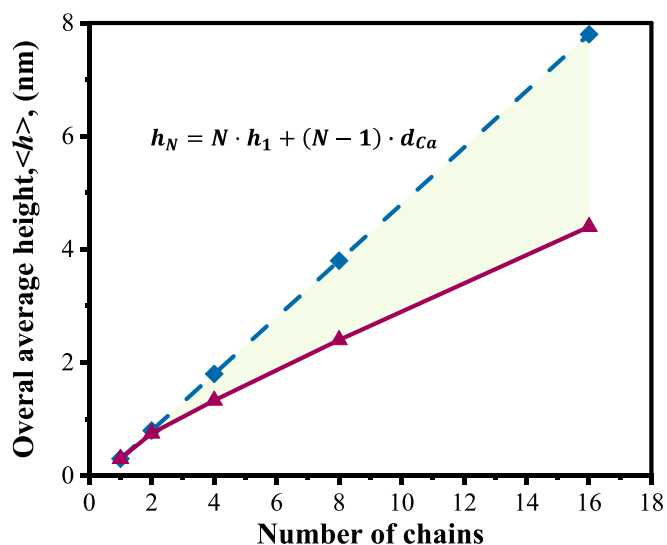
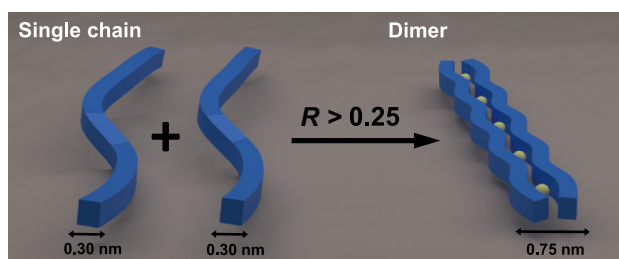


Fig. 7. Comparison of theoretical height values (broken line) and measured height values (solid line) for alginate egg-box structure with increasing number of chains. The theoretical values were calculated from the equation $h_N = Nh_1 + (N-1)d_{Ca}$, where h_1 is the height of single stranded chain and d_{Ca} is the diameter of Ca^{2+} .

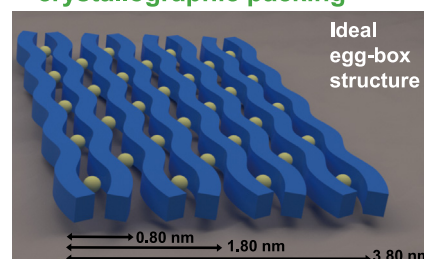
be seen from Fig. 6 that the Step II is dominated merely by the dimers without the presence of other assemblies, whereas the Step III sees the coexistence of the dimer-tetramer, tetramer-octamer, octamer-hexadecamer combinations, etc. This suggests that the dimerization is a more cooperative and critical process as compared with the subsequent multimerization process [10,11]. This phenomenon is interpretable by the specific nature of the coordination force that mediates the dimerization, relative to the non-specific nature of molecular interactions governing the subsequent lateral aggregation [9,15]. It has been well established that the pair of alginate chains in egg-box dimer is glued together by Ca^{2+} ions via specific coordination with O(2), O(3), O(61'), O(62'), and O(5') atoms.[43] However, the coordination of Ca^{2+} ions, for some reason, impairs the ability of dimers for lateral crystallographic packing.[9] Further lateral packing is thought to be mediated by disordered Na^+ and Ca^{2+} , water molecules, and hydrogen bonding, creating egg-box-compatible yet defected structure [9]. Compared with ALG56, ALG25 did not show the existence of octamer and hexadecamer at similar R . This should be due to the lower capability of lateral aggregation of ALG25 having lower G content and shorter G sequences.

Fig. 7 compares the theoretical and measured values of chain height for alginate egg-box structure with increasing number of chains. The deviation from the theoretical values is clearly enlarged with increasing number of chains. This should be due to the increased defects that are introduced with increasing lateral aggregation (Fig. 8). The egg-box dimers are formed by critical pairing of two guluronate sequences when at $R = 0.25$ for higher G alginate. This process is driven by specific coordination interaction between Ca^{2+} and guluronate units, and thus take places cooperatively in a zipper-like manner [11]. This results in ordered egg-box dimers, which serve as a structural basis for further growth and propagation (Fig. 8a). Further packing of the egg-box dimers by lateral aggregation is initialized when $R > 0.55$ (Fig. 8b). The lateral aggregation of two dimers into a tetramer is no longer mediated by coordination force, and instead involves disordered Ca^{2+} , Na^+ and H_2O molecules, etc. This introduces structural defects and gives rise to defected egg-box structure. The defected egg-box structure is in clear contrast to the ideal crystallographic structure shown in Fig. 8c, which requires strict structural regularity and alignment

(a) Critical dimerization mediated by specific coordination



(c) Ideal egg-box structure by crystallographic packing



(b) Lateral aggregation mediated by nonspecific interactions forming defected egg-box

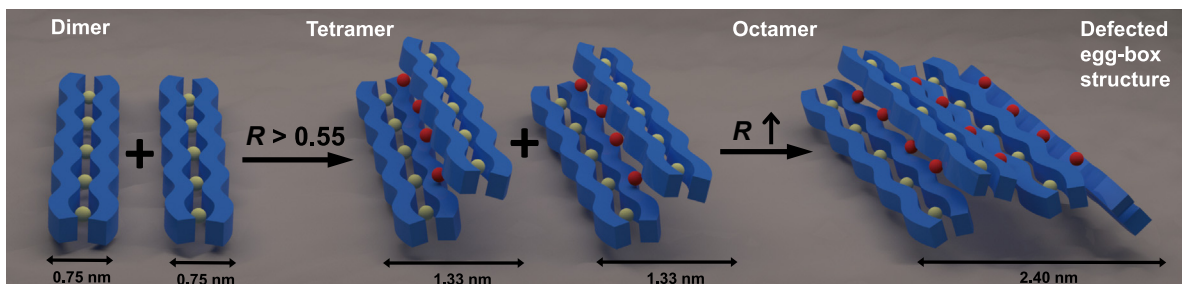


Fig. 8. 3D illustration of the formation of alginate egg-box structure by doubling growth: (a) critical dimerization of single chain via specific coordination; (b) doubling growth of dimers into tetramer, octamer, and even bigger defected egg-box multimer by lateral aggregation via nonspecific interactions. The yellow dots (●) represent specific coordinated Ca^{2+} ions, whereas the red dots (●) represent nonspecific ions including Na^+ and Ca^{2+} etc. Figure c shows an ideal egg-box structure formed by crystallographic packing of dimers, where the indicated dimension was derived from eq. (3). The dimension for single chain, dimer, tetramer, and octamer was obtained from AFM measurements. (For interpretation of the references to colour in this figure legend, the reader is referred to the web version of this article.)

for the side-by-side packing of dimers. Nonspecific interactions mediated by the disordered cations presumably require less structural regularity and allow more flexible orientation for the packing of dimers, and hence reduce the side-by-side spacing between two dimers. For instance, two dimers might partly overlap each other and/or align in different angles so that the overall measured width is reduced (Fig. 8b). This leads to a smaller width of the tetramer (1.33 nm), in comparison with that packed in a crystal (1.80 nm). Similarly, the doubling of tetramer into octamer at higher R , and likewise that into hexadecamer bring in more and more defects and thus produce bigger deviation from the ideal structure.

It should be pointed out that the model in Fig. 8 only aims to illustrate schematically the pathway of molecular assembly of alginate in a 3D space. A more precise determination of 3D structure of alginate aggregates is desired by using the techniques such as high-resolution wide-angle X-ray diffraction (WAXD) and cryogenic transmission electron microscopy (Cryo-TEM). Although the pathway of molecular assembly shown in Fig. 8 was obtained from dilute alginate system, it should shed light on the gelation behavior of alginate in concentrated solutions. For instance, the critical threshold of $R > 0.25$ for the dimerization of alginate chains could well explain the observed phenomenon that alginate solutions only gelled when $R > 0.25$ [14,15]. The effect of counterions on the gelation of alginate could also be well interpreted by the nonspecific interactions mediated lateral aggregation as shown in Fig. 8b [44].

8. Conclusions

The classic static egg-box model, developed for describing the gelation mechanism of an industrially important biopolymer alginate, failed to provide insights into the dynamic evolution and growth mode of alginate chains mediated by Ca^{2+} . Here, we unveiled for the first time a doubling growth mode for the formation of egg-box structure by using AFM in combination with poly-

mer statistical analysis. Alginate chains were found to pair into dimers in a critical and cooperative manner when $R(\text{Ca}/\text{G}) = 0.25$ for higher G alginate and 0.50 for lower G alginate. The formed egg-box dimers then acted as a structural basis for further lateral aggregation at higher R . Lateral aggregation was found to take place by successive doubling of dimers into tetramers, octamers and hexadecamers. The doubling growth created less ordered and more defected egg-box multimers, with increasing structural deviation from the ideal classic egg-box model. The deviation was attributed to the less critical and cooperative nature of the lateral aggregation mediated by nonspecific cations such as Na^+ and Ca^{2+} . The findings shed light on a long-standing debate regarding the pathway and mode of chain-chain association of alginate in the presence of Ca^{2+} and provided dynamic insight into the classic static egg-box model. Further studies are required to link the different states of molecular assembly with the macroscopic properties of alginate, e.g., gel properties.

CRediT authorship contribution statement

Yi Wang: Investigation, Writing – original draft. **Yiguo Zhao:** Investigation, Methodology, Data curation, Supervision. **Jun He:** Data curation, Visualization. **Cuixia Sun:** Formal analysis, Visualization. **Wei Lu:** Conceptualization. **Yin Zhang:** Resources, Writing – review & editing. **Yapeng Fang:** Conceptualization, Writing – review & editing, Project administration, Funding acquisition.

Data availability

Data will be made available on request.

Declaration of Competing Interest

The authors declare the following financial interests/personal relationships which may be considered as potential competing

interests: [Yapeng Fang reports financial support was provided by National Natural Science Foundation of China. Yapeng Fang reports financial support was provided by National Key Research and Development Project.].

Acknowledgement

The authors thank the financial supports from the National Natural Science Foundation of China (No. 31972023 and No. 32181240170) and the National Key Research and Development Project (2019YFD0901905).

Appendix A. Supplementary data

Supplementary data to this article can be found online at <https://doi.org/10.1016/j.jcis.2022.12.096>.

References

- [1] L. Cao, W. Lu, A. Mata, K. Nishinari, Y. Fang, Egg-box model-based gelation of alginate and pectin: A review, *Carbohydr. Polym.* 242 (2020) 116389.
- [2] G. Kopplin, A. Lervik, K.I. Draget, F.L. Aachmann, Alginate gels crosslinked with chitosan oligomers - a systematic investigation into alginate block structure and chitosan oligomer interaction, *RSC Adv.* 11 (2021) 13780.
- [3] C. Hu, W. Lu, A. Mata, K. Nishinari, Y. Fang, Ions-induced gelation of alginate: Mechanisms and applications, *Int. J. Biol. Macromol.* 177 (2021) 578–588.
- [4] G.T. Grant, E.R. Morris, D.A. Rees, P.J.C. Smith, D. Thom, Biological Interactions between Polysaccharides and Divalent Cations - Egg-Box Model, *FEBS Lett.* 32 (1973) 195.
- [5] E.R. Morris, D.A. Rees, D. Thom, J. Boyd, Chiroptical and Stoichiometric Evidence of a Specific, Primary Dimerization Process in Alginate Gelation, *Carbohydr. Res.* 66 (1978) 145.
- [6] D. Thom, G.T. Grant, E.R. Morris, D.A. Rees, Characterization of Cation Binding and Gelation of Polyuronates by Circular-Dichroism, *Carbohydr. Res.* 100 (1982) 29.
- [7] B.T. Stokke, K.I. Draget, O. Smidsrod, Y. Yuguchi, H. Urakawa, K. Kajiwara, Small-angle X-ray scattering and rheological characterization of alginate gels. 1. Ca-alginate gels, *Macromolecules* 33 (2000) 1853.
- [8] K.I. Draget, B.T. Stokke, Y. Yuguchi, H. Urakawa, K. Kajiwara, Small-angle x-ray scattering and rheological characterization of alginate gels. 3. Alginic acid gels, *Biomacromolecules* 4 (2003) 1661.
- [9] P. Sikorski, F. Mo, G. Skjak-Braek, B.T. Stokke, Evidence for egg-box-compatible interactions in calcium-alginate gels from fiber X-ray diffraction, *Biomacromolecules* 8 (2007) 2098.
- [10] Y. Fang, S. Al-Assaf, G.O. Phillips, K. Nishinari, T. Funami, P.A. Williams, L. Li, Multiple steps and critical behaviors of the binding of calcium to alginate, *J. Phys. Chem. B* 111 (2007) 2456.
- [11] Y. Fang, S. Al-Assaf, G.O. Phillips, K. Nishinari, T. Funami, P.A. Williams, Binding behavior of calcium to polyuronates: Comparison of pectin with alginate, *Carbohydr. Polym.* 72 (2) (2008) 334–341.
- [12] M. Borgogna, G. Skjak-Braek, S. Paoletti, I. Donati, On the Initial Binding of Alginate by Calcium Ions. The Tilted Egg-Box Hypothesis, *J. Phys. Chem. B* 117 (2013) 7277.
- [13] I. Donati, J. Benegas, S. Paoletti, On the Molecular Mechanism of the Calcium-Induced Gelation of Pectate, Different Steps in the Binding of Calcium Ions by Pectate, *Biomacromolecules* 22 (2021) 5000.
- [14] H. Liao, W. Ai, K. Zhang, M. Nakauma, T. Funami, Y. Fang, K. Nishinari, K.I. Draget, G.O. Phillips, Mechanisms of oligoguluronate modulating the calcium-induced gelation of alginate, *Polymer* 74 (2015) 166.
- [15] B. Zhang, B. Hu, M. Nakauma, T. Funami, K. Nishinari, K.I. Draget, G.O. Phillips, Y. Fang, Modulation of calcium-induced gelation of pectin by oligoguluronate as compared to alginate, *Food Res. Int.* 116 (2019) 232.
- [16] P.N. Depta, P. Gurikov, B. Schroeter, A. Forgács, J. Kalmár, G. Paul, L. Marchese, S. Heinrich, M. Dosta, DEM-Based Approach for the Modeling of Gelation and Its Application to Alginate, *J. Chem. Inf. Model.* 62 (2022) 49.
- [17] L. Schefer, J. Adamcik, R. Mezzenga, Unravelling Secondary Structure Changes on Individual Anionic Polysaccharide Chains by Atomic Force Microscopy**, *Angew. Chem. Int. Ed.* 53 (2014) 5376.
- [18] L. Schefer, I. Usov, R. Mezzenga, Anomalous Stiffening and Ion-Induced Coil-Helix Transition of Carrageenans under Monovalent Salt Conditions, *Biomacromolecules* 16 (2015) 985.
- [19] M. Diener, J. Adamcik, A. Sanchez-Ferrer, F. Jaedig, L. Schefer, R. Mezzenga, Primary, Secondary, Tertiary and Quaternary Structure Levels in Linear Polysaccharides: From Random Coil, to Single Helix to Supramolecular Assembly, *Biomacromolecules* 20 (2019) 1731.
- [20] M. Diener, J. Adamcik, J. Bergfreund, S. Catalini, P. Fischer, R. Mezzenga, Rigid Fibrillar Quaternary Structures Induced by Divalent Ions in a Carboxylated Linear Polysaccharide, *ACS Macro Lett.* 9 (2020) 115.
- [21] T. Funami, Y.P. Fang, S. Noda, S. Ishihara, M. Nakauma, K.I. Draget, K. Nishinari, G.O. Phillips, Rheological properties of sodium alginate in an aqueous system during gelation in relation to supermolecular structures and Ca(2+) binding, *Food Hydrocolloids* 23 (2009) 1746.
- [22] A.W. Decho, Imaging an alginate polymer gel matrix using atomic force microscopy, *Carbohydr. Res.* 315 (1999) 330.
- [23] K.A. Bowman, O.A. Aarstad, M. Nakamura, B.T. Stokke, G. Skjak-Braek, A.N. Round, Single molecule investigation of the onset and minimum size of the calcium-mediated junction zone in alginate, *Carbohydr. Polym.* 148 (2016) 52.
- [24] A.A. Solbu, A. Koernig, J.S. Kjesbu, D. Zaytseva-Zotova, M. Sletmoen, B.L. Strand, High resolution imaging of soft alginate hydrogels by atomic force microscopy, *Carbohydr. Polym.* 276 (2022) 118804.
- [25] H. Grasdalen, High-Field, H1-NMR Spectroscopy of Alginate-Sequential Structure and Linkage Conformations, *Carbohydr. Res.* 118 (1983) 255.
- [26] J. Adamcik, F. Valle, G. Witz, K. Rechendorff, G. Dietler, The promotion of secondary structures in single-stranded DNA by drugs that bind to duplex DNA: an atomic force microscopy study, *Nanotechnology* 19 (2008) 384016.
- [27] I. Usov, R. Mezzenga, FiberApp: An Open-Source Software for Tracking and Analyzing Polymers, Filaments, Biomacromolecules, and Fibrous Objects, *Macromolecules* 48 (2015) 1269.
- [28] M.B. Smith, H. Li, T. Shen, X. Huang, E. Yusuf, D. Vavylonis, Segmentation and tracking of cytoskeletal filaments using open active contours, *Cytoskeleton* 67 (2010) 693.
- [29] A. Bettini, M.R. Pozzan, E. Valdevit, C. Frontali, Microscopic persistence length of native DNA: Its relation to average molecular dimensions, *Biopolymers* 19 (1980) 1689.
- [30] A. Assifaoui, A. Lerbret, H.T.D. Uyen, F. Neiers, O. Chambin, C. Loupiac, F. Cousin, Structural behaviour differences in low methoxy pectin solutions in the presence of divalent cations (Ca²⁺ and Zn²⁺): a process driven by the binding mechanism of the cation with the galacturonate unit, *Soft Matter* 11 (2015) 551.
- [31] X. He, Y. Liu, H. Li, H. Li, Single-stranded structure of alginate and its conformational evolution after an interaction with calcium ions as revealed by electron microscopy, *RSC Adv.* 6 (2016) 114779.
- [32] F.G.A. Faas, B. Rieger, L.J. van Vliet, D.I. Cherny, DNA Deformations near Charged Surfaces: Electron and Atomic Force Microscopy Views, *Biophys. J.* 97 (2009) 1148.
- [33] H. Zhang, H. Wang, J. Wang, R. Guo, Q. Zhang, The effect of ionic strength on the viscosity of sodium alginate solution, *Polym. Adv. Tech.* 12 (2001) 740.
- [34] B. Maciel, C. Oelschlaeger, N. Willenbacher, Chain flexibility and dynamics of alginate solutions in different solvents, *Colloid Polym. Sci.* 298 (2020) 791.
- [35] I.M.N. Vold, K.A. Kristiansen, B.E. Christensen, A Study of the Chain Stiffness and Extension of Alginates, in Vitro Epimerized Alginates, and Periodate-Oxidized Alginates Using Size-Exclusion Chromatography Combined with Light Scattering and Viscosity Detectors, *Biomacromolecules* 7 (2006) 2136.
- [36] B.T. Stokke, D.A. Brant, The reliability of wormlike polysaccharide chain dimensions estimated from electron micrographs, *Biopolymers* 30 (1990) 1161.
- [37] C.K. Siew, P.A. Williams, N.W.G. Young, New insights into the mechanism of gelation of alginate and pectin: Charge annihilation and reversal mechanism, *Biomacromolecules* 6 (2005) 963.
- [38] E.D.T. Atkins, I.A. Nieduszynski, W. Mackie, K.D. Parker, E.E. Smolko, Structural components of alginic acid. I. The crystalline structure of poly-β-D-mannuronic acid. Results of X-ray diffraction and polarized infrared studies, *Biopolymers* 12 (1973) 1865.
- [39] E.D.T. Atkins, I.A. Nieduszynski, W. Mackie, K.D. Parker, E.E. Smolko, Structural components of alginic acid. II. The crystalline structure of poly-α-L-guluronic acid. Results of X-ray diffraction and polarized infrared studies, *Biopolymers* 12 (1973) 1879.
- [40] I. Braccini, R.P. Grasso, S. Pérez, Conformational and configurational features of acidic polysaccharides and their interactions with calcium ions: a molecular modeling investigation, *Carbohydr. Res.* 317 (1-4) (1999) 119–130.
- [41] I. Braccini, S. Perez, Molecular basis of Ca²⁺-induced gelation in alginates and pectins: The egg-box model revisited, *Biomacromolecules* 2 (2001) 1089.
- [42] Y. Marcus, Ionic radii in aqueous solutions, *Chem. Rev.* 88 (8) (1988) 1475–1498.
- [43] W. Mackie, S. Perez, R. Rizzo, F. Taravel, M. Vignon, Aspects of the conformation of polyguluronate in the solid state and in solution, *Int. J. Biol. Macromol.* 5 (1983) 329.
- [44] C. Hu, W. Lu, C. Sun, Y. Zhao, Y. Zhang, Y. Fang, Gelation behavior and mechanism of alginate with calcium: Dependence on monovalent counterions, *Carbohydr. Polym.* 294 (2022) 119788.